

Research Paper

PET Imaging of Integrin Positive Tumors Using ^{18}F Labeled Knottin Peptides

Shuanglong Liu^{1*}, Hongguang Liu^{1*}, Gang Ren¹, Richard H. Kimura², Jennifer R. Cochran², Zhen Cheng¹ 

1. Molecular Imaging Program at Stanford (MIPS), Bio-X Program, Department of Radiology, Stanford University, California, 94305-5344, USA
2. Molecular Imaging Program at Stanford (MIPS), Bio-X Program, and Department of Bioengineering, Stanford University, California, 94305-5344, USA

* S. Liu and H. Liu contributed equally to the work.

 Corresponding author: E-mail: zcheng@stanford.edu

© Ivyspring International Publisher. This is an open-access article distributed under the terms of the Creative Commons License (<http://creativecommons.org/licenses/by-nc-nd/3.0/>). Reproduction is permitted for personal, noncommercial use, provided that the article is in whole, unmodified, and properly cited.

Received: 2011.10.30; Accepted: 2011.12.17; Published: 2011.12.21

Abstract

Purpose: Cystine knot (knottin) peptides, engineered to bind with high affinity to integrin receptors, have shown promise as molecular imaging agents in living subjects. The aim of the current study was to evaluate tumor uptake and *in vivo* biodistribution of ^{18}F -labeled knottins in a U87MG glioblastoma model.

Procedures: Engineered knottin mutants 2.5D and 2.5F were synthesized using solid phase peptide synthesis and were folded *in vitro*, followed by radiolabeling with 4-nitrophenyl 2- ^{18}F -fluoropropionate (^{18}F -NFP). The resulting probes, ^{18}F -FP-2.5D and ^{18}F -FP-2.5F, were evaluated in nude mice bearing U87MG tumor xenografts using microPET and biodistribution studies.

Results: MicroPET imaging studies with ^{18}F -FP-2.5D and ^{18}F -FP-2.5F demonstrated high tumor uptake in U87MG xenograft mouse models. The probes exhibited rapid clearance from the blood and kidneys, thus leading to excellent tumor-to-normal tissue contrast. Specificity studies confirmed that ^{18}F -FP-2.5D and ^{18}F -FP-2.5F had reduced tumor uptake when co-injected with a large excess of the peptidomimetic c(RGDyK) as a blocking agent.

Conclusions: ^{18}F -FP-2.5D and ^{18}F -FP-2.5F showed reduced gallbladder uptake compared with previously published ^{18}F -FB-2.5D. ^{18}F -FP-2.5D and ^{18}F -FP-2.5F enabled integrin-specific PET imaging of U87MG tumors with good imaging contrasts. ^{18}F -FP-2.5D demonstrated more desirable pharmacokinetics compared to ^{18}F -FP-2.5F, and thus has greater potential for clinical translation.

Key words: Cystine knot peptide; RGD; Integrin; ^{18}F ; PET

Introduction

Angiogenesis, the formation of new blood vessels from preexisting vasculature, plays a critical role in tumor growth and metastasis [1-2]. To grow larger than 1–2 mm, a tumor needs sufficient blood flow, which provides oxygen and nutrients [3-4]. Integrins are a family of heterodimeric transmembrane receptors that are involved in multiple steps of tumor an-

giogenesis and metastasis. In particular, overexpression of integrins $\alpha_v\beta_3$, $\alpha_v\beta_5$, and $\alpha_5\beta_1$ is associated with malignancy and has been shown to play various roles in tumor growth and metastasis [5-8]. Thus, integrin receptors have been attractive targets for developing molecular probes for non-invasive tumor imaging using different modalities including magnetic reso-

nance imaging (MRI) [9], ultrasound [10-12], optical imaging [13-15], positron emission tomography (PET) [5, 16-18], and single-photon emission computed tomography (SPECT) [19-20].

Among the ligands that bind integrin receptors, arginine-glycine-aspartic acid (RGD)-containing peptides have been well validated for tumor imaging applications [21-22]. Radiofluorinated RGD probes such as ^{18}F -AH111585 and ^{18}F -Galacto-RGD are currently undergoing clinical studies in humans [16, 23-25]. In order to achieve higher tumor uptake, and better tumor-to-normal tissue contrasts, continued efforts to modify RGD-containing ligands remain an active area of research.

Cystine knots (also known as knottins) are small polypeptides with a common disulfide-bonded framework in which one disulfide bond threads through a macrocycle created by two other disulfide bonds and their connecting backbone segments [26-27], as illustrated in Figure 1A. As a result, knottins have a high degree of thermal and proteolytic stability and thus provide a valuable framework for development of targeting agents for *in vivo* applications [28-31]. Furthermore, the relatively small size of

knottins (~30-50 amino acids) makes them accessible by standard solid-phase peptide synthesis, and would result in fast blood clearance, which is desirable for molecular imaging applications.

Previously, high affinity integrin binding was conferred upon *Ecballium elaterium* trypsin inhibitor (EETI-II) using yeast surface display [32]. The 6-amino acid trypsin binding loop (PRILMR) of EETI-II was rationally substituted with an 11-amino-acid loop containing the RGD motif, and combinatorial methods were used to identify knottin mutants 2.5D and 2.5F, which bind to $\alpha_v\beta_3/\alpha_v\beta_5$ or $\alpha_v\beta_3/\alpha_v\beta_5/\alpha_5\beta_1$ integrins, respectively, with high (low nM) affinity [32-33]. The peptide sequences of knottins 2.5D and 2.5F are shown in Figure 1B. Subsequently, ^{64}Cu -labeled knottins were evaluated in mice bearing integrin-expressing U87MG glioblastoma xenografts, and microPET imaging and biodistribution studies showed rapid and high tumor accumulation, fast clearance from blood and normal organs, and low uptake in kidney and liver [33]. Overall, these studies demonstrated that engineered knottins are promising probes for molecular imaging applications.

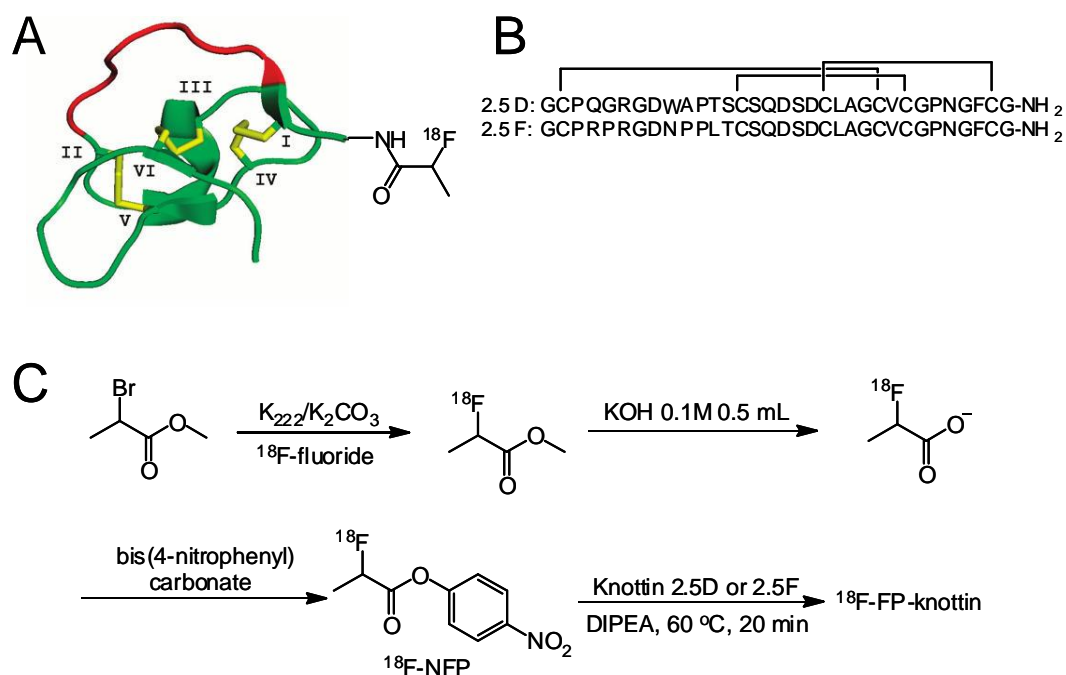


Figure 1 Schematic and sequences of knottin peptides. (A) Cartoon representation of a radiofluorinated knottin peptide scaffold. The imaging label ^{18}F -NFP was site-specifically conjugated to the N-terminus of the knottin. (B) Amino acid sequences of knottin peptides 2.5D and 2.5F with disulfide bonds between Cys1-Cys4, Cys2-Cy5, and Cys3-Cys6. (C) Synthetic scheme for ^{18}F -NFP synthon and knottin radiofluorination.

The physical properties of ^{18}F ($t_{1/2}$: 110 min, emits β^+ particles at an energy of 635 keV, 99% abundant) complement the high target binding affinity and rapid blood clearance of knottin peptides. Previously, we radiolabeled the knottin 2.5D with ^{18}F via the N-terminus of the peptide using *N*-succinimidyl-4- ^{18}F -fluorobenzoate (^{18}F -SFB), and showed that this conjugate, ^{18}F -FB-2.5D, could be used to image mice bearing U87MG tumor xenografts with good tumor-to-normal tissue contrast [34]. To improve knottin-based probes for PET imaging and facilitate their clinical translation, we evaluated the use of an alternative ^{18}F precursor, 4-nitrophenyl 2- ^{18}F -fluoropropionate (^{18}F -NFP), which has shown enhanced metabolic stability and reduced hydrophobicity [16, 35-36]. The resulting radio probes, ^{18}F -FP-2.5D and ^{18}F -FP-2.5F were evaluated for tumor uptake and tissue biodistribution in nude mice bearing U87MG tumor xenografts for comparison to our previous study.

Experimental Section

All commercially available materials were used as provided unless noted. All 9-fluorenylmethyloxycarbonyl (Fmoc) protected amino acids were purchased from Novabiochem/EMD Chemicals Inc (La Jolla, CA) or CS Bio (Menlo Park, CA). ^{125}I -labeled echistatin was purchased from GE Healthcare Life Sciences (Piscataway, NJ). All other chemicals were purchased from Fisher Scientific (Fair Lawn, NJ) unless otherwise specified. The U87MG human glioblastoma cell line was obtained from American Type Culture Collection (Manassas, VA). Nude mice (nu/nu) were purchased from Charles River Laboratory (Wilmington, MA). Semi-preparative reversed-phase high performance liquid chromatography (RP-HPLC), using a Vydac protein and peptide column (218TP510; 5 μm , 250 \times 10 mm), was performed on a Dionex 680 chromatography system with a UVD 170U absorbance detector and model 105S single-channel radiation detector (Carroll & Ramsey Associates). The recorded data were processed using Chromeleon version 7.1 software. With a flow rate of 5.0 mL/min, the mobile phase was changed from 95% solvent A [0.1% trifluoroacetic acid (TFA) in water] and 5% B [0.1% TFA in acetonitrile (MeCN)] (0–2 min) to 35% solvent A and 65% solvent B at 32 min. Analytical scale HPLC used the same gradient system except that the flow rate was 1.0 mL/min with a Vydac protein and peptide column (218TP510; 5 μm , 250 \times 4.6 mm). UV absorbance was monitored at 218 nm and the identification of the peptides was confirmed based on UV spectrum acquired using a photodiode array detector.

Instrumentation used for matrix-assisted laser desorption/ionization time of flight mass spectrometry (MALDI-TOF-MS) is the same as described in our previous publication [37].

Chemistry and Radiochemistry Peptides corresponding to the sequence of 2.5D and 2.5F were synthesized on a CS Bio CS036 Peptide Synthesizer (Menlo Park, CA) using Fmoc-based solid phase peptide synthesis. Briefly, Rink amide resin was swollen in *N,N*-dimethylformamide (DMF) for 30 min. Fmoc groups were removed with 20% piperidine in DMF. Aliquots of amino acids (1 mmol) were activated in a solution containing 1 mmol hydroxybenzotriazole (HOBt) and 0.5 M diisopropylcarbodiimide (DIC) in DMF. Following synthesis, side-chain deprotection and resin cleavage were achieved by addition of a 94:2.5:2.5:1 (v/v) mixture of TFA/triisopropylsilane/ethanedithiol/water for 2 h at room temperature. The crude product was precipitated with cold anhydrous ether, and purified using semi-preparative RP-HPLC. Peptide purity was analyzed by analytical scale RP-HPLC.

Large scale folding reactions were performed by incubating the linear peptide with 4 M guanidine, 10 mM reduced glutathione, 2 mM oxidized glutathione, and 0.5 M dimethyl sulfoxide (DMSO) at pH 7.5. The correctly folded peptide was separated from unfolded and partly folded peptides by RP-HPLC, where it appeared as a single peak with a shorter retention time than that of unfolded or misfolded precursors. Following purification, folded peptides 2.5D and 2.5F were lyophilized and stored at room temperature prior to use. Peptide purity and molecular masses were determined by analytical scale HPLC and MALDI-TOF-MS, respectively.

The synthesis of 4-nitrophenyl 2-fluoropropionate (^{19}F -NFP) is briefly described below. *Bis*(4-nitrophenyl) carbonate (15.2 mg, 50.0 μmol in 20 μL of diisopropylethylamine (DIPEA)) was added to a solution of 2-fluoropropionic acid (5.0 mg, 54.3 μmol in 200 μL of DMF). After incubating at 60 $^{\circ}\text{C}$ for 3 h, the reaction mixture was cooled to room temperature and diluted with 1 mL 5% acetic acid solution. The product ^{19}F -NFP was isolated by semi-preparative HPLC. The collected fractions were combined and the solvent was removed under reduced pressure. The product was obtained as white powder (5.9 mg, 56%). ESI-MS: m/z 213.1 [M] $^{+}$; ^1H NMR (CDCl_3 , 300 MHz): δ = 8.24 (d, J = 9.0 Hz, 2H), 7.27 (d, J = 9.0 Hz, 2H), 5.21 (m, 1H), 1.70 (dd, J = 6.8 Hz, 23.4 Hz, 3H). ^{13}C NMR (CDCl_3 , 75 MHz): δ = 18.9 (d, J = 22.5 Hz), 86.0 (d, J = 184.0 Hz), 122.9, 126.0, 146.4, 155.2, 168.5.

^{19}F -NFP labeled 2.5D and 2.5F (^{19}F -FP-2.5D,

¹⁹F-FP-2.5F) were prepared as reference standards. Briefly, 2.5D or 2.5F (0.5 mg, 0.15 μmol in 400 μL of DMSO) was mixed with ¹⁹F-NFP (0.3 mg, 1.5 μmol in 100 μL of DMSO and 10 μL of DIPEA) and reacted for 1 h at room temperature. The resulting conjugates, ¹⁹F-FP-2.5D and ¹⁹F-FP-2.5F were then purified by semi-preparative HPLC. Fractions containing the product were collected and lyophilized. The molecular masses of ¹⁹F-FP-2.5D and ¹⁹F-FP-2.5F were confirmed by MALDI-TOF-MS. Folded peptide 2.5D: m/z = 3244.0 for [MH]⁺ (C₁₂₉H₁₈₉N₄₀O₄₇S₆, calculated [MH]⁺ = 3244.5). Retention time on analytical scale HPLC is 16.2 min; Folded peptide 2.5F: m/z = 3292.1 for [MH]⁺ (C₁₃₁H₂₀₁N₄₂O₄₆S₆, calculated [MH]⁺ = 3292.6). Retention time: 15.2 min; ¹⁹F-FP-2.5D: m/z = 3317.5 for [MH]⁺ (C₁₃₂H₁₉₃FN₄₀O₄₈S₆, calculated [MH]⁺ = 3317.4). Retention time: 17.5 min; ¹⁹F-FP-2.5F: m/z = 3364.9 for [MH]⁺ (C₁₃₄H₂₀₃FN₄₂O₄₇S₆, calculated [MH]⁺ = 3365.3). Retention time: 18.3 min.

¹⁸F-NFP was prepared and used for knottin radiolabeling based on a previously reported procedure (Figure 1C) [38]. ¹⁸F-NFP (specific activity of 40–100 GBq/μmol at the end of synthesis, in 100 μL of DMSO) was added to the 2.5D or 2.5F peptide (100 μg) and 10 μL of DIPEA and reacted for 20 min at 60 °C. After adding 1 mL of water containing 50 μL of TFA to quench the reaction, the resulting conjugates were purified by semi-preparative HPLC using the same elution gradient as described for ¹⁹F-FP-knottin purification. The HPLC fractions containing ¹⁸F-FP-2.5D or ¹⁸F-FP-2.5F were collected, combined, and dried with a rotary evaporator. Radiolabeled peptides were reconstituted in PBS and sterilized using a 0.22 μm filter (Millipore) for *in vitro* and *in vivo* experiments.

Cell Culture: U87MG cells were cultured in DMEM containing high glucose (GIBCO, Carlsbad, CA), and supplemented with 10% fetal bovine serum (FBS) and 1% penicillin-streptomycin. Cells were expanded in tissue culture dishes and kept in a humidified atmosphere of 5% CO₂ at 37 °C, with media changes every other day. Confluent monolayers were detached with 0.05% Trypsin-EDTA, 0.01M PBS (pH 7.4) and dissociated into single-cell suspensions for further cell culture and experimentation.

U87MG Cell Binding Assay: Cell binding assays were performed as previously described [37, 39]. Briefly, 2 × 10⁵ U87MG cells were incubated with 0.06 nM ¹²⁵I-labeled echistatin and varying concentrations of peptides (2.5D, 2.5F, ¹⁹F-FP-2.5D or ¹⁹F-FP-2.5F) in integrin binding buffer [25 mM Tris pH 7.4, 150 mM NaCl, 2mM CaCl₂, 1 mM MgCl₂, 1 mM MnCl₂, and 0.1% bovine serum albumin (BSA)] at room temperature for 3 h. The cell-bound radioactivity remaining after washing was measured by gamma-counting.

Half-maximal inhibitory concentration (IC₅₀) values were determined by nonlinear regression using GraphPad Prism (GraphPad Software, Inc.). Experiments were performed with quadruplicate samples.

MicroPET Imaging: All animal studies were carried out in compliance with Federal and local institutional regulations for the conduct of animal experimentation. Approximately 10 × 10⁶ U87MG cells were suspended in 100 μL of PBS and subcutaneously implanted in the right shoulders of nude mice. Tumors were grown to a size of 0.5 cm in diameter (approximately 2–3 weeks). MicroPET scans were performed on a microPET R4 rodent model scanner (Concorde Microsystems Inc.). The scanner has a computer-controlled bed and 10.8-cm transaxial and 8-cm axial fields of view (FOVs). It has no septa and operates exclusively in the 3-dimensional (3D) list mode. Mice bearing U87MG xenografts were injected via tail vein with approximately 3.7 MBq (100 μCi) of ¹⁸F-FP-2.5D or ¹⁸F-FP-2.5F, with or without 10 mg/kg mouse body weight c(RGDyK). At 0.5, 1, and 2 h post injection (p.i.) mice were anesthetized with isoflurane (5% for induction and 2% for maintenance in 100% O₂). With the help of a laser beam attached to the scanner, mice were placed in the prone position and near the center of the field of view of the scanner where the image resolution and sensitivity is highest. Three minute static scans were obtained, and images were reconstructed by use of a 2-dimensional ordered-subsets expectation maximization (OSEM) algorithm. No background correction was performed. Region of interests (ROIs) were drawn over the tumor on decay-corrected whole-body coronal images. The maximum counts per pixel per minute were obtained from the ROI and converted to counts per milliliter per minute by using a calibration constant. Based on the assumption of a tissue density of 1 g/ml, ROIs were converted to counts per gram per min. The percent injected dose per gram of tissue (%ID/g) was determined by dividing counts per gram per minute by injected dose. No attenuation correction was performed.

Animal Biodistribution Studies: For biodistribution studies, nude mice bearing U87MG xenografts (n = 3 for each group) were injected via tail vein with approximately 3.7 MBq (100 μCi) of ¹⁸F-FP-2.5D or ¹⁸F-FP-2.5F, with or without 10 mg/kg mouse body weight c(RGDyK). Mice were sacrificed at 2 h p.i., and tumor and normal tissues of interest were removed and weighed, and their radioactivity was measured in a gamma-counter. The radioactivity uptake in the tumor and normal tissues was expressed as % ID/g.

Statistical Method: Statistical analysis was performed using the Student's *t*-test for unpaired data. A

95% confidence level was chosen to determine the significance between groups, with $P < 0.05$ being designated as significantly different.

Results

Chemistry and Radiochemistry: Peptides 2.5D and 2.5F were synthesized via solid phase peptide synthesis, followed by oxidative folding with a mixture of glutathione and DMSO. The final products were purified by semi-preparative RP-HPLC to achieve greater than 95% purity. Non-radioactive ^{19}F analogs were used as standards for radiosynthesis and for cell binding assays. ^{19}F -FP-2.5D and ^{19}F -FP-2.5F were prepared by direct conjugation of ^{19}F -NFP to knottin peptides 2.5D or 2.5F with yields of 92% and 95%, respectively. Product purities of greater than 95% were achieved as determined by analytical scale HPLC. MALDI-TOF-MS confirmed correct molecular masses for all peptides used in this study.

The total synthesis time for ^{18}F -NFP was approximately 100 min using a modified GE synthetic module (TRACERlab FX_{FN}) with decay corrected yields of $67 \pm 11\%$ ($n = 10$, Figure 1C) [36, 38]. The decay-corrected radiochemical yields of ^{18}F -FP-2.5D and ^{18}F -FP-2.5F based on ^{18}F -NFP were $12.0 \pm 2.7\%$ and $10.5 \pm 1.8\%$ ($n = 4$), respectively. The radiochemical purities of ^{18}F -FP-2.5D and ^{18}F -FP-2.5F were greater than 99% according to analytical scale HPLC. The specific radioactivity of ^{18}F -FP-2.5D and ^{18}F -FP-2.5F was estimated to be 20–40 GBq/ μmol at the end of synthesis.

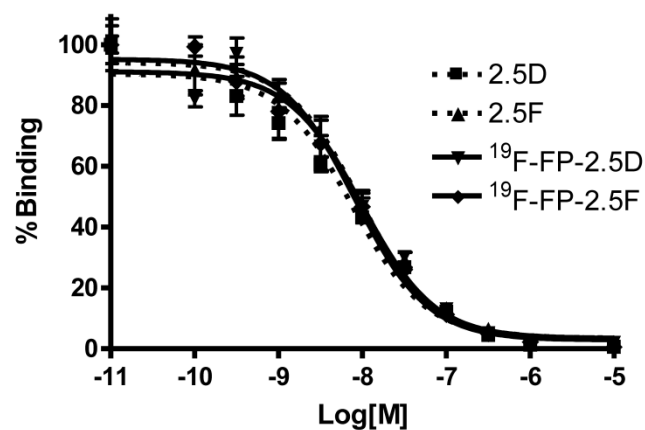


Figure 2 Competition binding of ^{125}I -echistatin to integrin receptors expressed on U87MG cells by 2.5D, 2.5F, ^{19}F -FP-2.5D, or ^{19}F -FP-2.5F. Results expressed as percentage of ^{125}I -echistatin binding are the mean of quadruplicate measurements \pm standard deviation. [M] = peptide molar concentration

In Vitro Cell Receptor-Binding Assay: Integrin positive U87MG human glioblastoma cells were used

for binding studies. Binding affinities of 2.5D, 2.5F, ^{19}F -FP-2.5D and ^{19}F -FP-2.5F were determined by competitive displacement of ^{125}I -echistatin, a potent integrin binder, from U87MG cells. All peptides inhibited the binding of ^{125}I -echistatin to U87MG cells in a concentration-dependent manner. The IC_{50} values for ^{19}F -FP-2.5D and ^{19}F -FP-2.5F were 7.4 ± 1.9 and 7.5 ± 1.3 nM, respectively ($n = 4$) (Figure 2). Comparison of binding values to unlabeled 2.5D and 2.5F (IC_{50} values = 6.9 ± 1.4 and 6.1 ± 1.6 nM, respectively) showed that fluoropropionate conjugation did not interfere with integrin receptor binding.

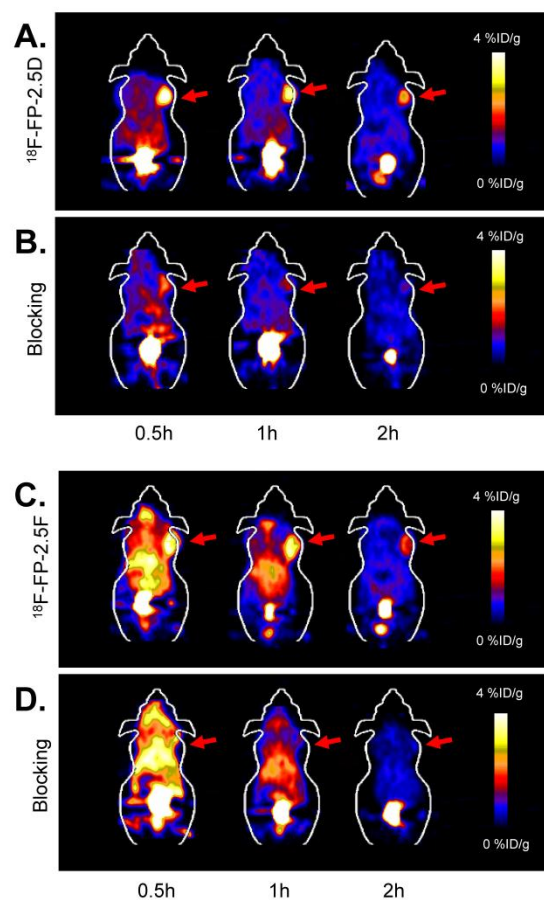


Figure 3 (A) and (C) Coronal microPET images of U87MG tumor-bearing mice at 0.5, 1, and 2 h post injection of approximately 3.7 MBq (100 μCi) of ^{18}F -FP-2.5D or ^{18}F -FP-2.5F, respectively. (B) and (D) Coronal microPET images of U87MG tumor-bearing mice at 0.5, 1, and 2 h after co-injection of approximately 3.7 MBq (100 μCi) of ^{18}F -FP-2.5D and ^{18}F -FP-2.5F with 10 mg c(RGDyK) per kg mouse body weight, respectively. Red arrows indicate tumors.

MicroPET Imaging Study: Static microPET scans were performed on U87MG tumor-bearing mice and representative decay-corrected coronal images at 0.5, 1, and 2 h after tail vein injection of ^{18}F -FP-2.5D or ^{18}F -FP-2.5F are shown in Figure 3 ($n = 3$ for each

group). U87MG tumors were clearly visualized, as both tracers produced excellent tumor-to-background contrast. MicroPET quantification of tumors and other organs was obtained from ROI analysis and the results at 0.5, 1, and 2 h p.i. are shown in Figure 4A and B. No significant difference in tumor uptake between these two probes was observed at each time point ($P > 0.05$). For ^{18}F -FP-2.5D, tumor uptake was 3.30 ± 1.08 , 2.86 ± 1.11 , and 2.37 ± 1.13 %ID/g at 0.5, 1, and 2 h p.i., respectively. For ^{18}F -FP-2.5F, tumor uptake was 3.74 ± 0.88 , 3.60 ± 0.25 , and 1.71 ± 0.37 %ID/g at 0.5, 1, and 2 h p.i., respectively. Both probes were cleared rapidly from the blood, and moderate to low renal retention was observed (4.24 ± 1.94 , 2.81 ± 1.42 , and 2.68 ± 2.90 %ID/g for ^{18}F -FP-2.5D at 0.5, 1, and 2 h p.i.; 13.39 ± 1.15 , 5.25 ± 0.65 , and 2.51 ± 0.16 %ID/g for ^{18}F -FP-2.5F at 0.5, 1, and 2 h p.i.). Interestingly, liver uptake of

^{18}F -FP-2.5F was significantly higher than ^{18}F -FP-2.5D at 0.5 h p.i., ($P < 0.05$), while no significant difference was observed at 1 h and 2 h p.i. Nonspecific uptake in the muscle was very low for both probes (0.51 ± 0.30 %ID/g and 0.44 ± 0.08 %ID/g for ^{18}F -FP-2.5D and ^{18}F -FP-2.5F at 2 h p.i., respectively). Gallbladder uptake of ^{18}F -FP-2.5D and ^{18}F -FP-2.5F was 0.86 ± 0.33 and 1.08 ± 0.41 %ID/g at 2 h p.i., respectively; these values were similar to background muscle uptake level. Tumor-to-normal tissues ratios of both probes at 0.5, 1, and 2 h were calculated and are shown in Figure 4C. At 0.5 h p.i., ^{18}F -FP-2.5D had higher tumor to liver, kidneys, and muscle ratios than those of ^{18}F -FP-2.5F ($P < 0.05$). This is consistent with the better tumor image quality of ^{18}F -FP-2.5D compared to ^{18}F -FP-2.5F at early time points (0.5 and 1 h p.i.), shown in Figure 3A and C.

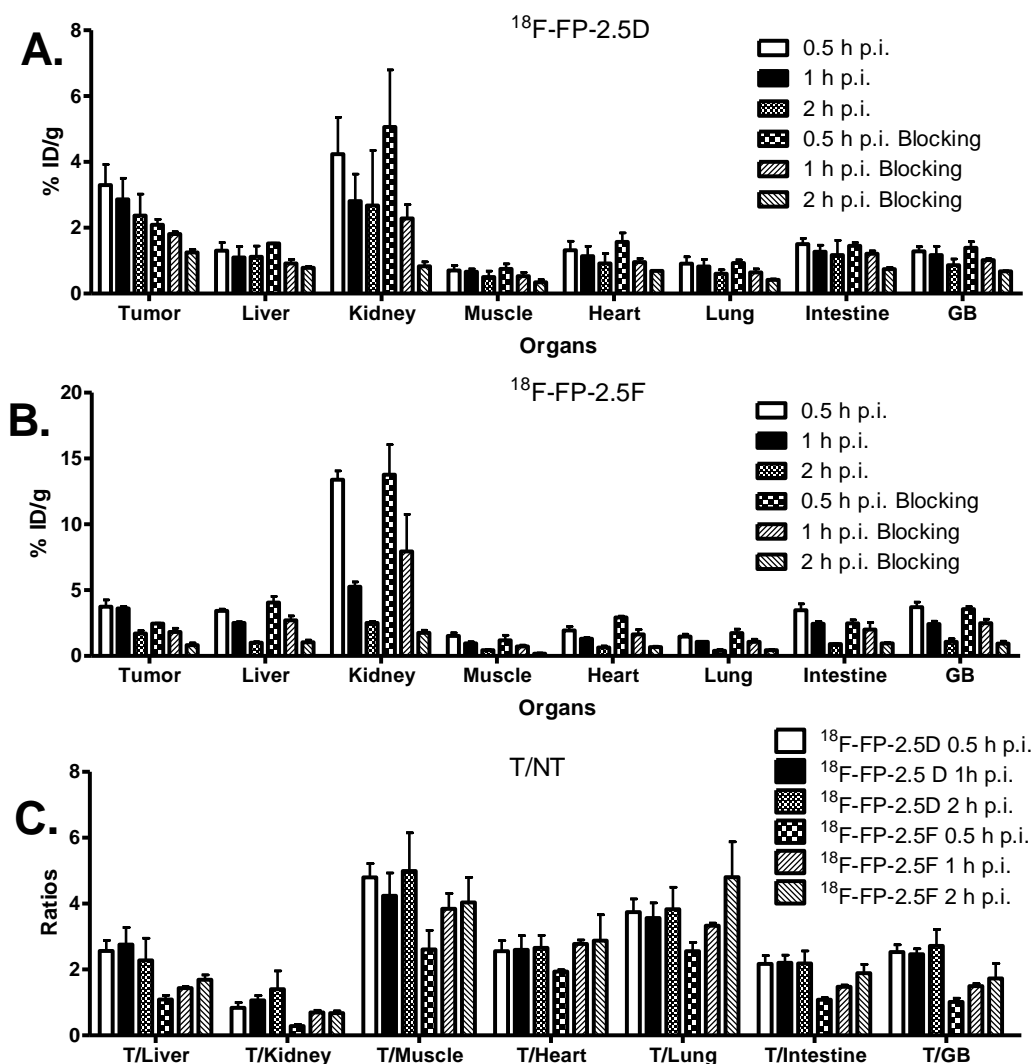


Figure 4 (A) and (B) MicroPET quantification results, expressed as %ID/g, in tumor and organs of U87MG xenograft models after intravenous injection of ~ 3.7 MBq ^{18}F -FP-2.5D or ^{18}F -FP-2.5F, respectively. (C) Tumor/nontumor (T/NT) ratios at 0.5, 1 and 2 h p.i. were calculated from A and B. GB = Gallbladder.

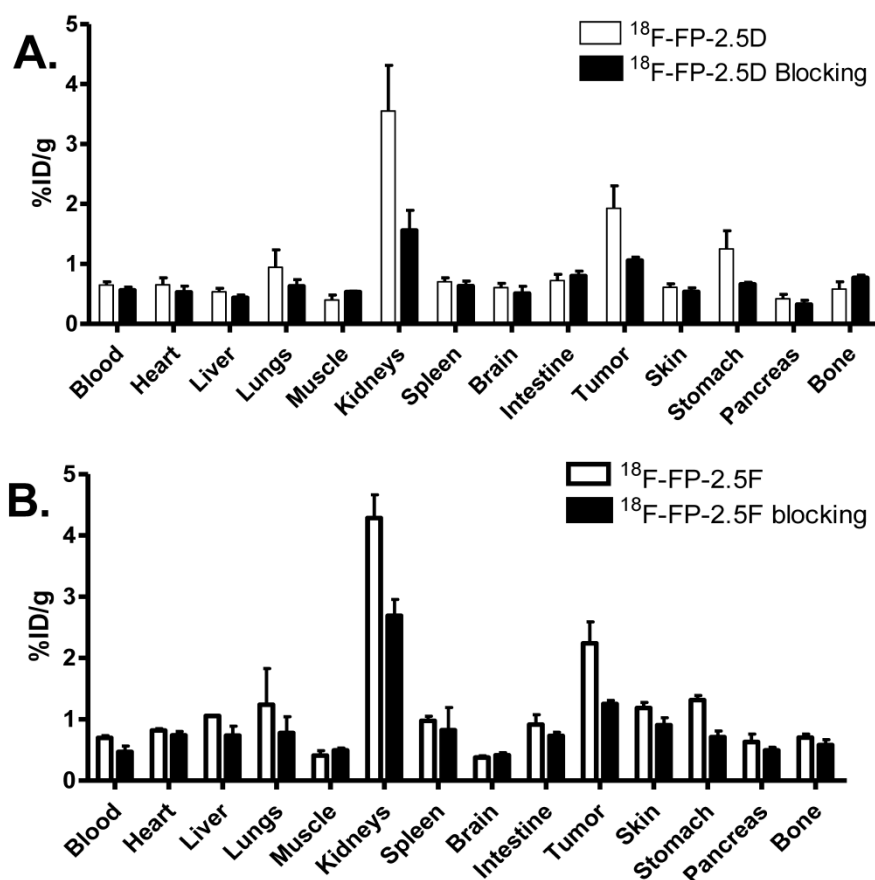


Figure 5 Biodistribution of ^{18}F -FP-2.5D or ^{18}F -FP-2.5F in U87MG tumor-bearing mice at 2 h after injection with or without co-injection of 10 mg/kg of c(RGDyK) as a blocking agent. Data are expressed as %ID/g \pm SD (n = 3 per group).

The integrin targeting specificity of both probes was demonstrated by co-injection of an excess of c(RGDyK) as a blocking agent. Figure 3B and D show the microPET images of ^{18}F -FP-2.5D and ^{18}F -FP-2.5F at 0.5, 1, and 2 h p.i. with co-injection of c(RGDyK). The corresponding microPET quantification results are shown in Figure 4. Coinjection of c(RGDyK) resulted in significant decreases in tumor uptake for both ^{18}F -FP-2.5D (3.91 ± 0.15 %ID/g without blocking *vs.* 1.96 ± 0.07 %ID/g with blocking, $P < 0.05$) and ^{18}F -FP-2.5F (3.83 ± 0.51 %ID/g without blocking *vs.* 1.90 ± 0.21 %ID/g with blocking, $P < 0.05$).

Biodistribution Studies: To validate microPET imaging experiments, biodistribution studies of ^{18}F -FP-2.5D and ^{18}F -FP-2.5F were performed at 2 h p.i. in U87MG xenograft models. Probe uptake in tumors and other major organs was calculated and is shown in Figure 5. No significant differences were observed compared to microPET image quantification. In these studies, the *in vivo* tumor targeting specificity of the probes was further confirmed by co-injection of an excess of c(RGDyK) blocking agent. A significant decrease in tumor uptake was observed for both

^{18}F -FP-2.5D (1.92 ± 0.65 %ID/g *vs.* 1.06 ± 0.10 %ID/g, $P < 0.05$) and ^{18}F -FP-2.5F (2.24 ± 0.60 %ID/g *vs.* 1.25 ± 0.10 %ID/g, $P < 0.05$) upon co-injection with c(RGDyK).

Discussion

Probe development is a central theme in cancer-specific molecular imaging applications. Historically, it has been challenging and time consuming to develop probes that bind tumor-related receptors with high affinity and specificity [40-42]. Numerous efforts have sought to generalize binder development using a variety of molecular platforms. Recently, small protein scaffolds have become robust starting points for molecular probe development [39, 43-44]. Knottins, which are generally 3-5 kDa in size, are highly stable scaffolds that have been shown to be amenable to rational and combinatorial engineering. Moreover, knottin engineering methods are maturing as new binders are being developed based on this versatile framework [30, 45]. Recently, high-affinity integrin-binding knottins were successfully identified by yeast display technology [32-33]. Radiolabeled

knottins, using ^{64}Cu or ^{18}F for PET imaging, have shown great promise for imaging integrin expression in mouse tumor models [31, 44, 46].

In this study, we evaluated ^{18}F -FP-labeled knottin 2.5D and 2.5F and explored potential advantages over ^{18}F -FB analogs, including effects on tumor uptake and retention and uptake in non-target organs. ^{18}F -fluoropropionate was chosen because it has relatively higher *in vivo* metabolic stability compared to ^{18}F -fluorobenzoate, as indicated by a high percentage of intact ^{18}F -FP-labeled probe in a metabolite analysis [38]. Moreover, ^{18}F -fluoropropionate is a less hydrophobic tag than that of ^{18}F -fluorobenzoate. Methods for radiosynthesis of ^{18}F -NFP have also been well established [38, 47-48]. Importantly, ^{18}F -NFP is practically the smallest ^{18}F -radiolabeling group for peptides, and is currently being used in clinical trials in human subjects [16, 23, 35].

Figure 4A and B show the results of microPET image quantification of ^{18}F -FP-2.5D and ^{18}F -FP-2.5F, which exhibit rapid tumor targeting and good tumor retention. Both probes exhibited maximum tumor uptake at 0.5 h p.i., and sustained tumor accumulation was observed. For example, at 1 and 2 h p.i., tumor uptake values were 2.86 ± 1.11 and 2.37 ± 1.13 %ID/g for ^{18}F -FP-2.5D, and 3.60 ± 0.25 and 1.71 ± 0.37 %ID/g for ^{18}F -FP-2.5F, respectively. Comparatively, the previously published knottin, ^{18}F -FB-2.5D demonstrated lower tumor uptake of 1.46 ± 0.35 %ID/g at 1 h p.i. [34]. Furthermore, gallbladder uptake was lower for ^{18}F -FP-2.5D (1.17 ± 0.47 %ID/g at 1 h p.i.), compared to ^{18}F -FB-2.5D (2.82 ± 1.31 %ID/g), which could be due to lower *in vivo* stability of ^{18}F -FB compared to ^{18}F -FP. For example, in a previous study, high *in vivo* stability was reported for a ^{18}F -FP labeled RGD dimer; more than 95% of the ^{18}F -labeled RGD dimer was shown to be intact at 2 h p.i. [38]. Importantly, ^{18}F -FP-2.5D had higher tumor-to-normal tissue ratios than ^{18}F -FB-2.5D, thus the ^{18}F -FP label resulted in improved imaging quality. Tumor-to-organ ratios for liver, kidneys, lungs, and gallbladder were 2.56 ± 0.55 , 0.83 ± 0.28 , 3.74 ± 0.70 , and 2.53 ± 0.39 , respectively, at 0.5 h p.i. for ^{18}F -FP-2.5D. In comparison, ratios for the same organs for ^{18}F -FB-2.5D were 1.97 ± 0.75 , 0.50 ± 0.16 , 2.03 ± 0.40 , and 0.71 ± 0.32 , respectively (Figure 4C). Collectively, these results highlight advantages of using a FP prosthetic group versus FB for knottin radiolabeling and *in vivo* imaging.

The IC_{50} values of knottin 2.5D and 2.5F indicated higher affinity integrin binding compared to that of a cyclic RGD pentapeptide (c(RGDyK)) published in the literature [49]; however, the tumor uptake for these probes were similar. For example, the U87MG tumor uptake of ^{18}F -FB labeled c(RGDyK)

was 2.56 ± 0.12 %ID/g [50], compared to tumor uptake values of 2.24 ± 0.60 %ID/g for ^{18}F -FP-2.5F at 2 h p.i. in the biodistribution study. These results indicate that the *in vivo* performance of a peptide-based molecular imaging probe depends on not only binding affinity, but other parameters such as charge, size, or hydrophobicity.

^{64}Cu -labeled knottin 2.5D and 2.5F analogs had similar tumor and normal tissue uptake, which resulted in comparable microPET contrast. However, different contrasts were observed for ^{18}F -FP-2.5D and ^{18}F -FP-2.5F (Figure 3A and C). ^{18}F -FP-2.5D showed better image quality compared to ^{18}F -FP-2.5F at 0.5 and 1 h p.i., but at a later time point (2 h p.i.), the tumor-to-muscle ratios for ^{18}F -FP-2.5D and ^{18}F -FP-2.5F reached the same level. Despite having similar binding affinities, the amino acid residues flanking the RGD motif in the engineered integrin binding loops of 2.5D and 2.5F are very different (Figure 1B), which may have influenced their *in vivo* behavior in this study. These results further indicate the importance of evaluating different radiolabeling methods in order to optimize the *in vivo* performance of protein- or peptide-based imaging probes.

PET provides a sensitive technique to identify and characterize disease in living systems. For a newly-developed PET probe to be successfully translated into the clinic, it should have high tumor uptake with reasonable tumor-to-background ratios in support of clinical radioisotopes with relatively short half-lives, such as ^{18}F . The PET probe should also be able to be prepared in high radiochemical yield, purity, and specific activity. The total radiosynthesis time for ^{18}F -FP-2.5D and ^{18}F -FP-2.5F was approximately 100 minutes. Furthermore, the ^{18}F -FP labeled knottins developed here meet some of these basic criteria such as high labeling yield, high *in vivo* stability, high radiochemical purity and good tumor uptake with high tumor-to-background ratios. Together, these results suggest that ^{18}F -FP-2.5D, and potentially ^{18}F -FP-2.5F, may have clinical potential for integrin imaging.

In conclusion, radiolabeled knottin peptides, ^{18}F -FP-2.5D and ^{18}F -FP-2.5F showed integrin-specific PET imaging of U87MG tumors marked by good contrast, fast tumor targeting, rapid clearance from body and relatively low uptake in normal tissues. The ^{18}F -FP-labeled knottin mutant 2.5D exhibited higher tumor-to-normal tissue contrast compared to ^{18}F -FB-2.5D, perhaps due to increased *in vivo* stability of ^{18}F -FP residue. Taken together, these results suggest that ^{18}F -FP-2.5D may perform well in clinical applications.

Acknowledgments

This work was supported, in part, by the National Cancer Institute (NCI) 5R01 CA119053 (ZC), and the V Foundation for Cancer Research (JRC). The Stanford University cyclotron team is acknowledged for ^{18}F production.

Conflict of Interest

The authors have declared that no conflict of interest exists.

References

- Beer AJ, Kessler H, Wester HJ, Schwaiger M. PET Imaging of Integrin $\alpha_v\beta_3$ Expression. *Theranostics*. 2011; 1: 48-57.
- Folkman J. Role of angiogenesis in tumor growth and metastasis. *Semin Oncol*. 2002; 29: 15-8.
- Folkman J. Seminars in Medicine of the Beth Israel Hospital, Boston. Clinical applications of research on angiogenesis. *N Engl J Med*. 1995; 333: 1757-63.
- Sharma RA, Harris AL, Dalglish AG, Steward WP, O'Byrne KJ. Angiogenesis as a biomarker and target in cancer chemoprevention. *Lancet Oncol*. 2001; 2: 726-32.
- Bello L, Francolini M, Marthyn P, Zhang J, Carroll RS, Nikas DC, et al. $\alpha_v\beta_3$ and $\alpha_v\beta_5$ integrin expression in glioma periphery. *Neurosurgery*. 2001; 49: 380-9.
- Friedlander M, Brooks PC, Shaffer RW, Kincaid CM, Varner JA, Chershan DA. Definition of two angiogenic pathways by distinct α_v integrins. *Science*. 1995; 270: 1500-2.
- Horton MA. The $\alpha_v\beta_3$ integrin "vitronectin receptor". *Int J Biochem Cell Biol*. 1997; 29: 721-5.
- Millard M, Odde S, Neamati N. Integrin targeted therapeutics. *Theranostics*. 2011; 1: 154-88.
- Schmieder AH, Winter PM, Caruthers SD, Harris TD, Williams TA, Allen JS, et al. Molecular MR imaging of melanoma angiogenesis with $\alpha_v\beta_3$ -targeted paramagnetic nanoparticles. *Magn Reson Med*. 2005; 53: 621-7.
- Dayton PA, Pearson D, Clark J, Simon S, Schumann PA, Zutshi R, et al. Ultrasonic analysis of peptide- and antibody-targeted microbubble contrast agents for molecular imaging of $\alpha_v\beta_3$ -expressing cells. *Mol Imaging*. 2004; 3: 125-34.
- Ellegala DB, Leong-Poi H, Carpenter JE, Klibanov AL, Kaul S, Shaffrey ME, et al. Imaging tumor angiogenesis with contrast ultrasound and microbubbles targeted to $\alpha_v\beta_3$. *Circulation*. 2003; 108: 336-41.
- Leong-Poi H, Christiansen J, Klibanov AL, Kaul S, Lindner JR. Noninvasive assessment of angiogenesis by ultrasound and microbubbles targeted to α_v -integrins. *Circulation*. 2003; 107: 455-60.
- Achilefu S, Bloch S, Markiewicz MA, Zhong T, Ye Y, Dorshow RB, et al. Synergistic effects of light-emitting probes and peptides for targeting and monitoring integrin expression. *Proc Natl Acad Sci U S A*. 2005; 102: 7976-81.
- Chen X, Conti PS, Moats RA. In vivo near-infrared fluorescence imaging of integrin $\alpha_v\beta_3$ in brain tumor xenografts. *Cancer Res*. 2004; 64: 8009-14.
- Wang W, Ke S, Wu Q, Charnsangavej C, Gurfinkel M, Gelovani JG, et al. Near-infrared optical imaging of integrin $\alpha_v\beta_3$ in human tumor xenografts. *Mol Imaging*. 2004; 3: 343-51.
- Haubner R, Weber WA, Beer AJ, Vabulienė E, Reim D, Sarbia M, et al. Noninvasive visualization of the activated $\alpha_v\beta_3$ integrin in cancer patients by positron emission tomography and [^{18}F]Galacto-RGD. *PLoS Med*. 2005; 2: e70.
- Li ZB, Chen K, Chen X. ^{68}Ga -labeled multimeric RGD peptides for microPET imaging of integrin $\alpha_v\beta_3$ expression. *Eur J Nucl Med Mol Imaging*. 2008; 35: 1100-8.
- Li ZB, Wu Z, Chen K, Chin FT, Chen X. Click chemistry for ^{18}F -labeling of RGD peptides and microPET imaging of tumor integrin $\alpha_v\beta_3$ expression. *Bioconjug Chem*. 2007; 18: 1987-94.
- Janssen ML, Oyen WJ, Dijkgraaf I, Massuger LF, Frielink C, Edwards DS, et al. Tumor targeting with radiolabeled $\alpha_v\beta_3$ integrin binding peptides in a nude mouse model. *Cancer Res*. 2002; 62: 6146-51.
- Sadeghi MM, Krassilnikova S, Zhang J, Gharaei AA, Fassaei HR, Esmailzadeh L, et al. Detection of injury-induced vascular remodeling by targeting activated $\alpha_v\beta_3$ integrin in vivo. *Circulation*. 2004; 110: 84-90.
- Shi J, Zhou Y, Chakraborty S, Kim YS, Jia B, Wang F, et al. Evaluation of In-Labeled Cyclic RGD Peptides: Effects of Peptide and Linker Multiplicity on Their Tumor Uptake, Excretion Kinetics and Metabolic Stability. *Theranostics*. 2011; 1: 322-40.
- Lang L, Li W, Jia HM, Fang DC, Zhang S, Sun X, et al. New Methods for Labeling RGD Peptides with Bromine-76. *Theranostics*. 2011; 1: 341-53.
- Beer AJ, Grosu AL, Carlsen J, Kolk A, Sarbia M, Stangier I, et al. [^{18}F]Galacto-RGD positron emission tomography for imaging of $\alpha_v\beta_3$ expression on the neovasculature in patients with squamous cell carcinoma of the head and neck. *Clin Cancer Res*. 2007; 13: 6610-6.
- Beer AJ, Haubner R, Sarbia M, Goebel M, Luderschmidt S, Grosu AL, et al. Positron emission tomography using [^{18}F]Galacto-RGD identifies the level of integrin $\alpha_v\beta_3$ expression in man. *Clin Cancer Res*. 2006; 12: 3942-9.
- Kenny LM, Coombes RC, Oulie I, Contractor KB, Miller M, Spinks TJ, et al. Phase I trial of the positron-emitting Arg-Gly-Asp (RGD) peptide radioligand ^{18}F -AH111585 in breast cancer patients. *J Nucl Med*. 2008; 49: 879-86.
- Chiche L, Heitz A, Gelly JC, Gracy J, Chau PT, Ha PT, et al. Squash inhibitors: from structural motifs to macrocyclic knottins. *Curr Protein Pept Sci*. 2004; 5: 341-9.
- Pallaghy PK, Nielsen KJ, Craik DJ, Norton RS. A common structural motif incorporating a cystine knot and a triple-stranded β -sheet in toxic and inhibitory polypeptides. *Protein Sci*. 1994; 3: 1833-9.
- Craik DJ, Daly NL, Waite C. The cystine knot motif in toxins and implications for drug design. *Toxicon*. 2001; 39: 43-60.
- Kolmar H. Alternative binding proteins: biological activity and therapeutic potential of cystine-knot miniproteins. *FEBS J*. 2008; 275: 2684-90.
- Kolmar H. Biological diversity and therapeutic potential of natural and engineered cystine knot miniproteins. *Curr Opin Pharmacol*. 2009; 9: 608-14.
- Kolmar H. Engineered cystine-knot miniproteins for diagnostic applications. *Expert Rev Mol Diagn*. 2010; 10: 361-8.
- Kimura RH, Levin AM, Cochran FV, Cochran JR. Engineered cystine knot peptides that bind $\alpha_v\beta_3$, $\alpha_v\beta_5$, and $\alpha_5\beta_1$ integrins with low-nanomolar affinity. *Proteins*. 2009; 77: 359-69.
- Kimura RH, Cheng Z, Gambhir SS, Cochran JR. Engineered knottin peptides: a new class of agents for imaging integrin expression in living subjects. *Cancer Res*. 2009; 69: 2435-42.
- Miao Z, Ren G, Liu H, Kimura RH, Jiang L, Cochran JR, et al. An engineered knottin peptide labeled with ^{18}F for PET imaging of integrin expression. *Bioconjug Chem*. 2009; 20: 2342-7.
- Beer AJ, Haubner R, Goebel M, Luderschmidt S, Spilker ME, Wester HJ, et al. Biodistribution and pharmacokinetics of the $\alpha_v\beta_3$ -selective tracer ^{18}F -galacto-RGD in cancer patients. *J Nucl Med*. 2005; 46: 1333-41.
- Haubner R, Kuhnast B, Mang C, Weber WA, Kessler H, Wester HJ, et al. [^{18}F]Galacto-RGD: synthesis, radiolabeling, metabolic

- stability, and radiation dose estimates. *Bioconjug Chem.* 2004; 15: 61-9.
37. Cheng Z, Zhang L, Graves E, Xiong Z, Dandekar M, Chen X, et al. Small-animal PET of melanocortin 1 receptor expression using a ^{18}F -labeled α -melanocyte-stimulating hormone analog. *J Nucl Med.* 2007; 48: 987-94.
 38. Liu S, Liu Z, Chen K, Yan Y, Watzlowik P, Wester HJ, et al. ^{18}F -Labeled Galacto and PEGylated RGD Dimers for PET Imaging of $\alpha_v\beta_3$ Integrin Expression. *Mol Imaging Biol.* 2010; 12:530-8.
 39. Cheng Z, De Jesus OP, Namavari M, De A, Levi J, Webster JM, et al. Small-animal PET imaging of human epidermal growth factor receptor type 2 expression with site-specific ^{18}F -labeled protein scaffold molecules. *J Nucl Med.* 2008; 49: 804-13.
 40. Li Z, Conti PS. Radiopharmaceutical chemistry for positron emission tomography. *Adv Drug Deliv Rev.* 2010; 62: 1031-51.
 41. Miller JC, Thrall JH. Clinical molecular imaging. *J Am Coll Radiol.* 2004; 1: 4-23.
 42. Serdons K, Verbruggen A, Bormans GM. Developing new molecular imaging probes for PET. *Methods.* 2009; 48: 104-11.
 43. Jiang L, Kimura RH, Miao Z, Silverman AP, Ren G, Liu H, et al. Evaluation of a ^{64}Cu -labeled cystine-knot peptide based on agouti-related protein for PET of tumors expressing $\alpha_v\beta_3$ integrin. *J Nucl Med.* 2010; 51: 251-8.
 44. Miao Z, Levi J, Cheng Z. Protein scaffold-based molecular probes for cancer molecular imaging. *Amino Acids.* 2010; 21: 947-54.
 45. Moore SJ, Cochran JR. Engineering Knottins as Novel Binding Agents. *Methods Enzymol.* 2012; 503: 223-51.
 46. Moore SJ, Leung CL, Cochran JR. Knottins: Disulfide-bonded Therapeutic and Diagnostic Peptides. *Drug Discovery Today: Technologies.* 2011; doi:10.1016/j.ddtec.2011.07.003.
 47. Liu S, Shen B, Chin FT, Cheng Z. Recent Progress in Radiofluorination of Peptides for PET Molecular Imaging. *Curr Org Synth.* 2011; 8: 584-92.
 48. Block D, Coenen HH, Stocklin G. Nca F-18-Fluoroacylation Via Fluorocarboxylic Acid-Esters. *J Labelled Compd Rad.* 1988; 25: 185-200.
 49. Chen X, Hou Y, Tohme M, Park R, Khankaldyyan V, Gonzales-Gomez I, et al. Pegylated Arg-Gly-Asp peptide: ^{64}Cu labeling and PET imaging of brain tumor $\alpha_v\beta_3$ -integrin expression. *J Nucl Med.* 2004; 45: 1776-83.
 50. Chen X, Park R, Hou Y, Khankaldyyan V, Gonzales-Gomez I, Tohme M, et al. MicroPET imaging of brain tumor angiogenesis with ^{18}F -labeled PEGylated RGD peptide. *Eur J Nucl Med Mol Imaging.* 2004; 31: 1081-9.